

Article

# Copper Tricomponent Catalysts Application for Hydrogen Production from Ethanol

Łukasz Hamryszak <sup>1,\*</sup>, Maria Kulawska <sup>1</sup>, Maria Madej-Lachowska <sup>2,\*</sup>, Michał Śliwa <sup>3</sup>, Katarzyna Samson <sup>3</sup> and Małgorzata Ruggiero-Mikołajczyk <sup>3</sup>

<sup>1</sup> Institute of Chemical Engineering, Polish Academy of Sciences, 5 Bałtycka Street, 44-100 Gliwice, Poland; maria.kulawska@gmail.com

<sup>2</sup> Department of Biosystem Engineering and Chemical Processes, Opole University of Technology, 31 Sosnkowskiego Street, 45-272 Opole, Poland

<sup>3</sup> Jerzy Haber Institute of Catalysis and Surface Chemistry, Polish Academy of Sciences, 8 Niezapominajek Street, 30-239 Krakow, Poland; ncsliva@cyf-kr.edu.pl (M.Ś.); ncsamson@cyf-kr.edu.pl (K.S.); nbruggie@cyf-kr.edu.pl (M.R.-M.)

\* Correspondence: lukasz.hamryszak@iich.gliwice.pl (Ł.H.); m.madej-lachowska@po.edu.pl (M.M.-L.); Tel.: +48-32-231-0811 (Ł.H.); +48-77-449-8774 (M.M.-L.)

**Abstract:** The application of copper-based catalysts in the production of pure hydrogen in the steam reforming of ethanol was performed. The tricomponent Cu/Zr catalysts with about 4 mass% addition of nickel, cobalt, or cerium have been prepared in our laboratory. The properties of obtained catalysts were compared with bimetallic Cu/Zr catalyst prepared and tested according to the same procedure. Catalytic tests were carried out in the continuous flow fixed-bed reactor in the wide temperature range of 433–593 K for initial molar ratio of ethanol to water equal to 1:3. Catalysts were characterized by XRD, TPR, CO<sub>2</sub>-TPD, and TPO methods. Cu/Zr/Ce catalyst proved to be the best; hydrogen yield reached the value of 400 L/(kg<sub>cat</sub>·h), selectivity towards carbon monoxide was below 0.5% and the one towards methane was not detected. Additions of Ni or Co did not bring significant improvement in activity.

**Keywords:** copper–zirconium catalysts; ethanol steam reforming; hydrogen fuel cells; hydrogen production; non-noble metal catalysts



**Citation:** Hamryszak, Ł.; Kulawska, M.; Madej-Lachowska, M.; Śliwa, M.; Samson, K.; Ruggiero-Mikołajczyk, M. Copper Tricomponent Catalysts Application for Hydrogen Production from Ethanol. *Catalysts* **2021**, *11*, 575. <https://doi.org/10.3390/catal11050575>

Academic Editors: Anna Gancarczyk, Przemysław Jodłowski and Maciej Sitarz

Received: 26 February 2021

Accepted: 28 April 2021

Published: 30 April 2021

**Publisher's Note:** MDPI stays neutral with regard to jurisdictional claims in published maps and institutional affiliations.



**Copyright:** © 2021 by the authors. Licensee MDPI, Basel, Switzerland. This article is an open access article distributed under the terms and conditions of the Creative Commons Attribution (CC BY) license (<https://creativecommons.org/licenses/by/4.0/>).

## 1. Introduction

The rising energy production in all developed and developing countries causes the corresponding increase in the environment pollution. New restrictions and regulations require new clean technologies of high efficiency of energy generation [1]. Hydrogen is considered as a carrier of clean energy. Many methods of hydrogen production have been developed. The industrial production of hydrogen is currently carried out in the process of gasification of coal and other fossil materials, in the process of steam reforming of hydrocarbons (mainly methane), oxygenates (mainly methanol) [2,3], and from water electrolysis [4]. Many attempts have been made in recent decades to produce hydrogen from ethanol or bioethanol derived from any source of starch [5]. In the process of ethanol steam reforming (ESR) hydrogen is a product of highly endothermic catalytic reaction [6]:



Besides this main reaction, many side and consecutive reactions occur, giving undesired by-products, e.g., carbon monoxide, methane, acetic acid, acetaldehyde, ethene, and others:





Various stages of this process depend on process parameters and catalysts used [7,8].

To deal with such a complex process, the complicated catalytic systems with improved selectivity to hydrogen have been developed. The biggest problem is developing high resistance to carbon deposition on the catalyst surface and, at the same time, minimalization of carbon monoxide formation. Carbon monoxide is a strong poison that deactivates the proton exchange membrane fuel cell (PEMFC) catalyst. The system of low temperature PEMFC cannot accept more than 10 ppm for efficient operation, while high-temperature PEMFC tolerates supply of gas containing up to 5 vol.% of CO [8].

Early investigations on ESR catalysts were focused on application of noble metals as main component of catalysts: rhodium, platinum, ruthenium, lanthanum, or iridium [9–16]. These catalysts were characterized by high resistance to deactivation, selectivity towards hydrogen in the range of 60–75% and content of the CO in the product below 10%. Unfortunately, the level of CO is too high for an application in fuel cells. Additionally, due to the high production cost of these types of catalysts, many new studies have been conducted to replace them with cheaper ones.

First experiments were carried out on bimetallic systems based on nickel [17–27] and cobalt [17,20,21,27–30], there are also some experiments with copper [7,17,21,24,31] and cerium [27,32] as base metal; the second component was alumina or zirconia. Later, there were attempts on improving activity of bimetallic catalysts by addition of another component. The base component was nickel: Ni/CeO<sub>2</sub>–Al<sub>2</sub>O<sub>3</sub>, Ni/CeO<sub>2</sub>–La<sub>2</sub>O<sub>3</sub>, Ni/La<sub>2</sub>O<sub>3</sub>–Al<sub>2</sub>O<sub>3</sub>, Ni/La<sub>2</sub>O<sub>3</sub>–ZrO<sub>2</sub> [33–35], Ni<sub>0.95</sub>Mo<sub>0.05</sub>/SBA–15 [36], Ni/ZnO/Al<sub>2</sub>O<sub>3</sub> [37,38], Ni<sub>3</sub>Mg<sub>2</sub>/AlO<sub>y</sub> [39], and Ni–Cu/CeMnO<sub>2</sub> [40]. Dan et al. [33] found that additional oxides of Ce or La to Ni/Zr and Ni/Al catalysts gave a 25–45% increase in hydrogen yield at temperature of 593 K, and methane was the only byproduct (selectivity above 20%). Montero et al. [34], investigating the catalytic system of Ni/La<sub>2</sub>O<sub>3</sub>–Al<sub>2</sub>O<sub>3</sub>, found an important increase in hydrogen yield (from 10% to 90%) and lower coking, following increase in temperature (from 873 to 973 K). La-doped ceria-supported nickel catalyst Ni–CeLa<sub>0.2</sub> revealed complete conversion and high H<sub>2</sub> production in Xiao et al. [35] investigations, where catalyst was prepared by sol–gel method. In experiments of Kim et al. [36], addition of molybdenum to Ni/SBA–15 catalyst caused an increase in hydrogen selectivity from 65% to 79% and prolonged catalyst lifetime. Barroso et al. [37] found that increase in Ni content (from 1 to 25 mass%) not only increases activity of Ni/Zn/Al catalyst but also increases CO selectivity (from 11% to 58%) at temperature of 773 K. Anjaneyulu et al. [38] experimented with Zn/Al ratio (changing it from 1:2 to 2:1) in Ni/ZnO/Al<sub>2</sub>O<sub>3</sub> catalyst and showed better Ni dispersion and coking resistance for Zn/Al ratio 2:1. Very stable catalyst Ni<sub>3</sub>Mg<sub>2</sub>/AlO<sub>y</sub>, working at very low temperature of 573 K, with about 60% hydrogen selectivity and lack of CO, was formed by Fang team's [39]. Tricomponent catalysts Ni/CeMnO<sub>2</sub> promoted by Cu, Co, K, and Fe were tested by Sohrabi et al. [40]. Cu addition (Ni–Cu/CeMnO<sub>2</sub>, 5.3–3.6/44/21, mass%) increased conversion from 57% to 70%, the highest H<sub>2</sub> yield (60%) was obtained using Fe addition (Ni–Fe/CeMnO<sub>2</sub>, 6.3–2.8/27/26), but CO level was still high.

There were some works concerning copper-based trimetallic catalysts: Cu/Al<sub>2</sub>O<sub>3</sub>/Mn [41], CuO/ZrO<sub>2</sub>/Me (Me = Ni, Mn, Ga) [42], Cu/Zr/Ni [24], Cu/Ni/Me (Me = Ce, Nb, Si) [43,44], Cu/Ce/Al [8], and Cu/Ce/Zr [45]. Activity of these types of catalysts was investigated in a wide range of temperatures (573–1073 K) and substrate ratios (ethanol/water ratio equal to 1:30–1:3). According to Das et al. [41], copper-based catalysts, as dehydrogenation catalysts, were most effective for maximizing hydrogen production in ESR process. The team led by Das studied ethanol steam reforming process in the presence of Cu/Al<sub>2</sub>O<sub>3</sub> catalysts promoted with manganese. Maximum ethanol conversion of 60.7% and hydrogen yield of

3.74 (mol H<sub>2</sub>/mol ethanol converted) were observed at temperature of 633 K over catalyst with 2.5 mass% Mn loading, at ethanol/water ratio equal to 1:6 [41]. Dong et al. [45] investigated the effect of four preparation methods: sol-gel, co-precipitation, one-step impregnation, and two-step impregnation on activity of Cu/Ce/Zr (1/9/1 metal ratio) catalysts in carbon monoxide removal from gas rich in hydrogen. They found the best co-precipitation method, with Na<sub>2</sub>CO<sub>3</sub> as precipitant, at calcination temperature of 773 K. Śliwa and Samson [42] used CuO/ZrO<sub>2</sub> catalysts doped with Mn, Ni, or Ga in ESR process. The reaction parameters were as follows: temperature of 623 K, ethanol/water ratio equal to 1:10, CuO/ZrO<sub>2</sub> ratio equal to 2.3 mass%/mass%, and the concentration of dopants was 5 mass%. The maximum hydrogen yield, 52% of the stoichiometric ethanol efficiency value, was achieved by the addition of nickel. However, it was accompanied with 17% selectivity to CO. Bergamaschi et al. [24] found that addition of 6 mass% of nickel to Cu/Zr catalyst increased specific surface area BET and hydrogen selectivity at 573 K. Dancini-Pontes et al. [43] found that Cu/Ni/CeO<sub>2</sub> catalyst revealed much higher resistance to deactivation and better efficiency at temperature of about 723 K, in comparison with Cu/Ni system. The presence of nitrogen in reaction mixture increased hydrogen selectivity of about 20–30% after 8 h reaction course at temperature of 723 K. Snytnikov et al. [8] achieved nearly 20% increase in hydrogen selectivity and only about 2% CO content in the product at relatively low temperature of 623 K by an addition of γ-Al<sub>2</sub>O<sub>3</sub> to CuO/CeO<sub>2</sub> catalyst.

The properties of these catalysts depend mainly not only on their composition, especially on active metal content, but also on the parameters of preparation. Activity and lifetime of a catalyst can be improved by a method of preparation. Chen et al. [44] obtained nearly twice an increase in hydrogen yield by significantly lowering the temperature of reduction with hydrogen (from 923 to 623 K) of CuNi/SiO<sub>2</sub> catalyst.

The literature data indicate that improvements in catalyst activity and resistance to deactivation can be achieved by introducing a third component, changing the ratio of individual elements in the catalyst, activation parameters, preparation method, and even the composition of the reaction mixture. However, it is difficult to say which of the catalysts presented in the literature was the best because their activities were usually tested under different, often not fully specified conditions, and their activity parameters were also different.

The aim of the presented work was to obtain an active and selective catalyst for hydrogen production in ethanol steam reforming by introducing Ni, Co, or Ce additives to a Cu/Zr binary catalyst studied previously [17].

## 2. Results and Discussion

### 2.1. Characteristics of the Catalysts

The phase composition of the catalysts after hydrogen reduction was determined by XRD. The XRD patterns of the catalysts after hydrogen reduction are presented in Figure 1.

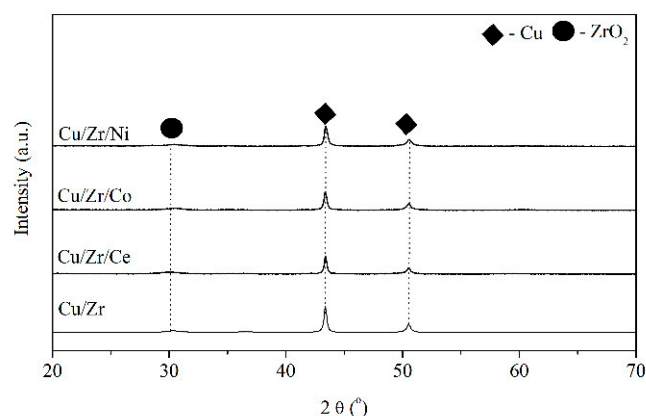


**Figure 1.** XRD patterns of tested catalysts after hydrogen reduction.

In the obtained XRD patterns (Figure 1), the Cu<sup>0</sup> ( $2\theta = 43, 51^\circ$ ) and ZrO<sub>2</sub> ( $2\theta = 30^\circ$ ) phases are present. The intensity of XRD peaks related with metallic copper are higher in comparison with XRD peak assigned to ZrO<sub>2</sub>. This may be caused by the different concentration of these two phases and differences in the crystallite sizes. On the other hand, there are no XRD peaks related to the CoO, NiO, and CeO<sub>2</sub> phases in the diffractograms. The lack of these signals can be due to high dispersion of additives in the synthesized catalysts. The crystallite sizes calculated by Scherrer method are presented in Table 1.

**Table 1.** Composition, textural properties, and size of crystallites of tested catalysts.

Catalyst	CuO (mass%)	ZrO <sub>2</sub> (mass%)	Other Metal Oxides <sup>a</sup> (mass%)	Size of Crystallites <sup>b</sup> (nm)		S <sub>Cu</sub> <sup>c</sup> (m <sup>2</sup> /g <sub>Cu</sub> )	S <sub>BET</sub> <sup>d</sup> (m <sup>2</sup> /g)	V <sub>p</sub> (cm <sup>3</sup> /g)	D <sub>p</sub> (nm)	D <sub>Cu</sub> (%)
				Cu <sup>0</sup> (111)	ZrO <sub>2</sub> (111)					
Cu/Zr/Ni	63.3	32.7	4	37.8	6.3	13	40	0.14	13	2.0
Cu/Zr/Co	63.3	32.7	4	32.8	5.6	11	32	0.12	15	1.7
Cu/Zr/Ce	63.3	32.7	4	75.0	4.7	6	35	0.13	15	0.9
Cu/Zr	63.8	36.2	–	23.1	5.5	3	23	0.07	13	0.5

<sup>a</sup> Co<sub>3</sub>O<sub>4</sub>, NiO, and CeO; <sup>b</sup> after hydrogen reduction; <sup>c</sup> measured by dissociative N<sub>2</sub>O adsorption; <sup>d</sup> measured by N<sub>2</sub> adsorption at 77 K.

The crystallite sizes of Cu<sup>0</sup> are larger than others. Large crystallites of copper revealed low dispersion that ranges from 2% for Cu/Zr/Ni catalyst and 1.7% for Cu/Zr/Co to 0.9% for Cu/Zr/Ce [7].

Experimental adsorption and desorption isotherms of nitrogen (77 K) are presented in Figure 2a. The investigated catalysts reveal mesopore structure with homogeneous pore distribution, which is characteristic for capillary condensation typical for the mesopore range. This is supported by the shape of the isotherms, which are of type IV (according to IUPAC classification) with hysteresis loops of type H1 for all tested catalysts (cylindrical pores of almost constant cross-section) (Figure 2a) [46]. Moreover, this is in line with the pore volume distribution profiles exhibiting single narrow peaks with maximum at 4 nm (Figure 2b).

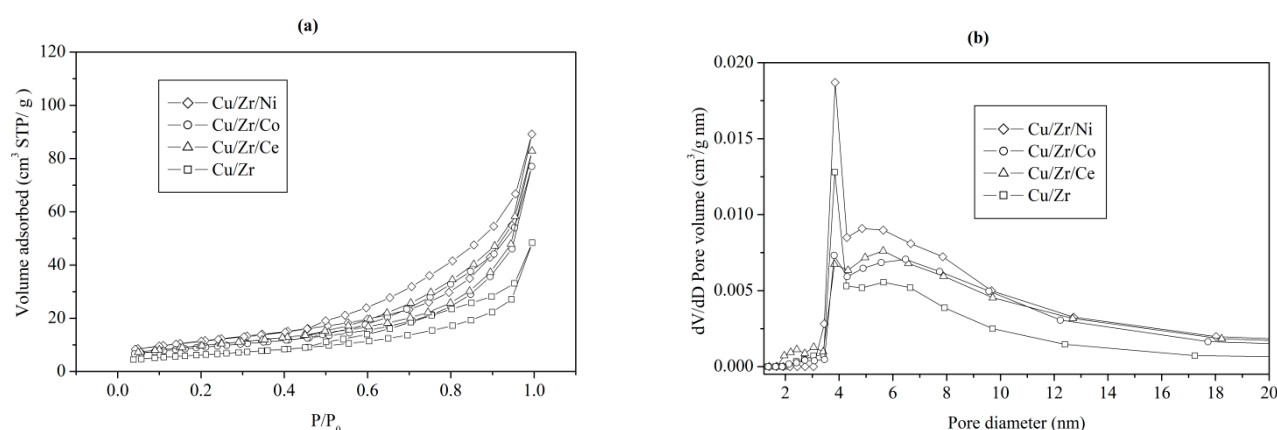


**Figure 2.** (a) N<sub>2</sub> adsorption/desorption isotherms (77 K) and (b) pore size distribution of the catalysts.

Cu/Zr and Cu/Zr/Ni catalysts have much more mesoporous structure compared with Cu/Zr/Co and Ce/Zr/Ce catalysts. The copper surface area (S<sub>Cu</sub>), specific surface area BET (S<sub>BET</sub>), pore volume (V<sub>p</sub>), and average pore diameter (D<sub>p</sub>) are presented in Table 1. An addition of an oxide of Ce, Co, or Ni to Cu/Zr catalyst results in about 60–70% increase in S<sub>Cu</sub> and S<sub>BET</sub> values followed by V<sub>p</sub> increase in the following order: Cu/Zr < Cu/Zr/Co < Cu/Zr/Ce < Cu/Zr/Ni. The total pore volume of obtained catalysts reaches about 0.14 cm<sup>3</sup>/g.

H<sub>2</sub>-TPR profiles of investigated catalysts are presented in Figure 3. The peaks were observed within the temperature range of 540–583 K. The observed single reduction peak

refers solely to the reduction of CuO to Cu<sup>0</sup>. The addition of Ni or Co or Ce oxides to the Cu/Zr catalyst resulted in a 16–40° decrease in the temperature corresponding to the maximum reduction rate ( $T_{max}$ ) indicating that the dopants (Ni, Co and Ce) facilitate the reduction of CuO [47,48]. An addition of Co oxide to Cu/Zr catalyst causes decrease in the temperature corresponding to maximum reduction ( $T_{max}$ ) rate by 40 K. Similar effect was observed for others dopants, but in this case, shift in  $T_{max}$  was only by ca. 20 K.

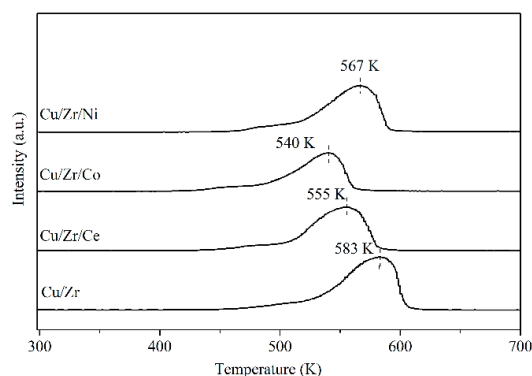


**Figure 3.** Temperature-programmed reduction of H<sub>2</sub>(H<sub>2</sub>-TPR) profiles of tested catalysts.

The CO<sub>2</sub>-TPD experiments were performed in order to evaluate the surface basicity of the synthesized catalysts. The recorded TPD profiles (Figure 4) were analyzed in the temperature range corresponding with temperature profiles at which the steam reforming of ethanol reaction had been carried out.

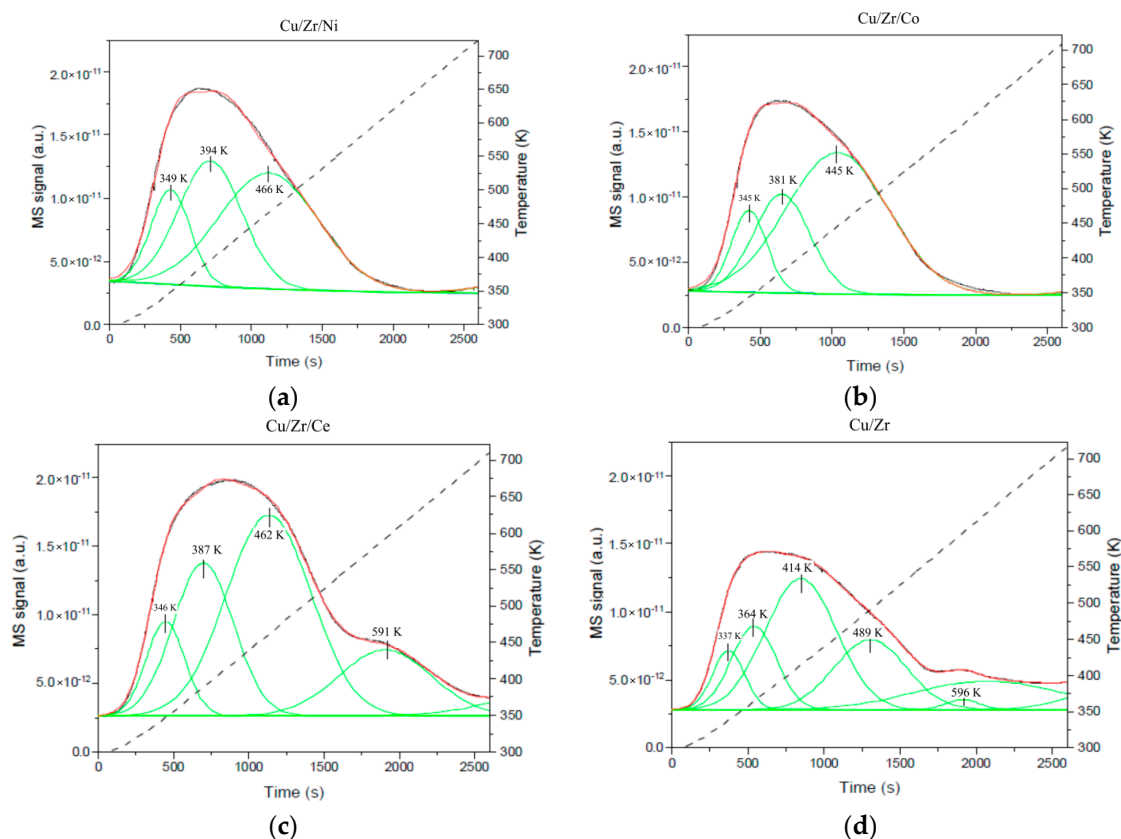


**Figure 4.** CO<sub>2</sub> temperature-programmed desorption (CO<sub>2</sub>-TPD) profiles for (a) Cu/Zr/Ni, (b) Cu/Zr/Co, (c) Cu/Zr/Ce and (d) Cu/Zr: signal—black line, cumulative curve—red line, deconvoluted peaks used for quantification—green line, temperature—dashed line. (For interpretation of the references to color in this figure legend, the reader is referred to the Web version of this article).

For all catalysts, the very broad and complex desorption profile is observed with overlapping signals. In order to get insight in the distribution of weak, medium, and strong basic sites, the TPD profiles were deconvoluted into Gaussian peaks. Based on the maxima position of deconvoluted peaks, signals were assigned accordingly to desorption of CO<sub>2</sub> from weak (323–423 K), medium (423–513 K), and strong (>513 K) basic sites. Only deconvoluted maxima up to 623 K were used for the calculation of basic sites concentration (Table 2), since this was the final calcination temperature of catalysts.

**Table 2.** Quantitative analysis of basic sites for synthesized catalysts.

Catalyst	Basic Sites (μmol/g)			Amount of CO <sub>2</sub> Adsorbed (μmol)	Amount of CO <sub>2</sub> Desorbed (μmol)	Total Basicity (μmol/g)
	Weak	Medium	Strong			
CuZrNi	40.4	39.6	–	3.9	4.0	79.9
CuZrCo	25.1	42.8	–	3.3	3.3	67.9
CuZrCe	34.2	45.4	16.4	5.1	4.9	96.0
CuZr	41.3	13.9	1.0	2.9	2.8	56.2

The maxima that were used for quantitative analysis are marked in the TPD profiles. In the case of all catalysts, the amount of adsorbed CO<sub>2</sub> and desorbed CO<sub>2</sub> during TPD experiments is the same, meaning that the entire CO<sub>2</sub> was desorbed during TPD runs in the analyzed temperature range. According to quantitative results (Table 2), the lowest concentration of basic sites is observed for Cu/Zr (56.2 μmol/g). In the case of this catalyst, the contribution of weak basic sites in total basicity is the highest among synthesized samples (41.3 μmol/g). On the other hand, the modification of Cu/Zr catalysts with dopants leads to increase in total surface basicity in the following order of Cu/Zr/Co < Cu/Zr/Ni < Cu/Zr/Ce. According to literature [49,50] weak basic sites can be related with surface hydroxyl group, medium basic sites with Zr<sup>4+</sup>–O<sup>2-</sup> pairs, and the strong basic sites with the low-coordination oxygen anions.

Additionally, the distribution of basic sites for modified catalysts changes in comparison with Cu/Zr. The decrease in concentration of weak basic sites is visible upon catalyst modification with Co and Ce, whereas concentration of weak basic sites decreases. Moreover, in the case of Cu/Zr/Ce, strong basic sites are generated (16.4 μmol/g). For catalyst doped with Ni, the amount of medium basic sites is higher when compared with Cu/Zr but there is no change in concentration of weak basic sites.

## 2.2. Catalytic Activity

Catalytic activity results are graphically presented in Figures 5–8.

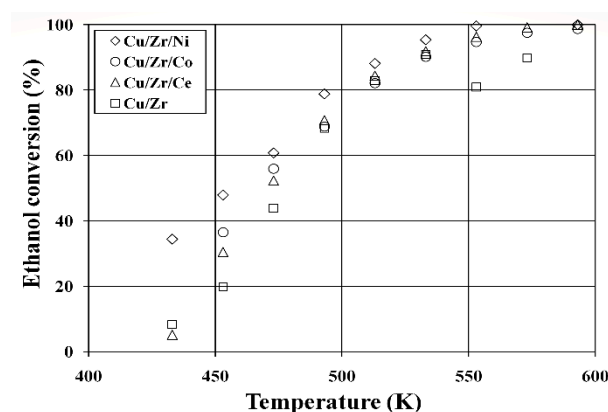


**Figure 5.** The effect of temperature on ethanol conversion in ethanol steam reforming (ESR) over tested catalysts.

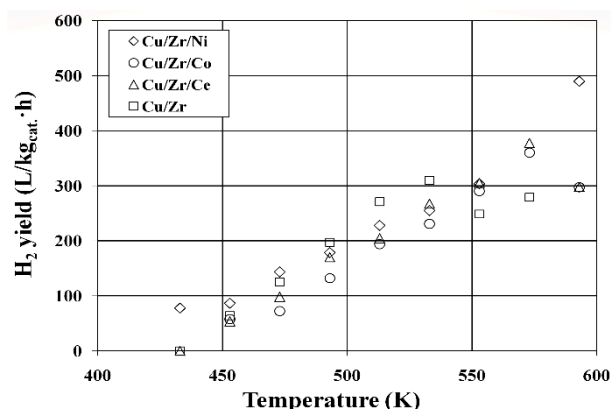


Figure 6. The effect of temperature on H<sub>2</sub> yield in ESR over tested catalysts.

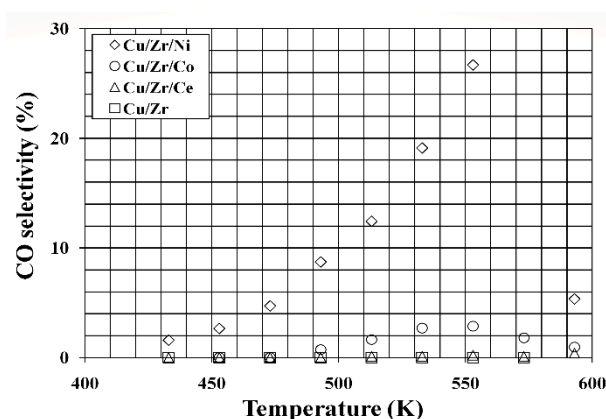


Figure 7. The effect of temperature on CO selectivity in ESR over tested catalysts.

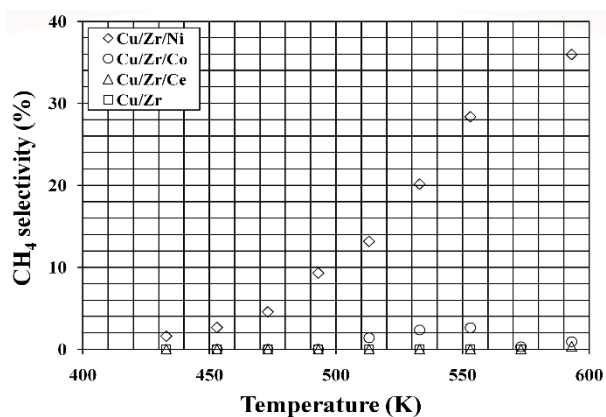


Figure 8. The effect of temperature on CH<sub>4</sub> selectivity in ESR over tested catalysts.

All modified catalysts reached about 100% conversion of ethanol (see Figure 5), a slightly higher than basic Cu/Zr catalyst (~90% conversion). The temperature effected the hydrogen yield (see Figure 6) in similar way up to temperature of 550 K, giving the value of 300 L/(kg<sub>cat</sub>·h). In the presence of Cu/Zr/Ni catalyst, further increase in temperature caused the highest increase in hydrogen yield, resulting in the value of 490 L/(kg<sub>cat</sub>·h) (Table 3); unfortunately accompanied by high production of carbon monoxide (see Figure 7, Table 3), harmful for fuel cells—27% selectivity at 553 K and rapid decrease to 6% selectivity at 593 K. The methane selectivity also reached high value of 36% at 593 K (see Figure 8 and Table 3), but it is not harmful, methane could potentially be used as a source of energy in this endothermic ethanol steam reforming process.

**Table 3.** Maximum hydrogen yield at corresponding temperature for tested catalysts.

Catalyst	$W_{H_2}^{max}$ (L/kg <sub>cat</sub> ·h)	T (K)	$\alpha$ (%)	$S_{CO}$ (%)	$S_{CH_4}$ (%)
Cu/Zr/Ni	490	593	100	5.3	35.9
Cu/Zr/Co	360	573	97	1.8	0.3
Cu/Zr/Ce	378	573	99	0.1	0.0
Cu/Zr	309	533	91	0.0	0.0

Cu/Zr/Co and Cu/Zr/Ce catalysts revealed similar properties. The hydrogen yield reached similar values, with maximum of about 380 L/(kg<sub>cat</sub>·h) at 573 K (Table 3). Selectivity towards carbon monoxide was low, with a maximum of 3% at 553 K for Cu/Zr/Co catalyst; very low value, below 0.5% for Cu/Zr/Ce catalyst. Baneshi et al. [51] also confirmed such a good selectivity of the cerium-containing catalyst. Methane was not detected in the course of reaction in the presence of Cu/Zr/Ce catalyst, whereas in the presence of Cu/Zr/Co catalyst, it was 3% at temperature of 553 K.

The Cu/Zr/Ni catalyst, which has the highest value of  $S_{Cu}$  (13 m<sup>2</sup>/g<sub>Cu</sub>),  $D_{Cu}$  (2%), and  $S_{BET}$  (40 m<sup>2</sup>/g), exhibited the highest yield to hydrogen (490 L/(kg<sub>cat</sub>·h). On the other hand, Cu/Zr/Co catalyst, whose physicochemical properties are close to Cu/Zr/Ni catalyst, yields the lower value of hydrogen (about 300 L/(kg<sub>cat</sub>·h), similar to Cu/Zr/Ce (Table 1 and Figure 7).

According to XRD analysis, the Cu/Zr/Co catalyst has large CuO crystallites and the smallest ZrO<sub>2</sub> crystallites. This is in agreement with the chemisorption of N<sub>2</sub>O, which showed that the Cu/Zr/Ce catalyst has low value of metallic copper dispersion and metallic coppers surface area (Table 1) resulting from agglomeration of copper crystallite. This can lead to lower hydrogen yield [52]. Additionally, similar value of hydrogen yield is observed for Cu/Zr/Co catalyst, having the same average pore diameter as Cu/Zr/Ce catalyst. Mastalir et al. [53] in their investigation on methanol steam reforming found that the changes of copper concentration in Cu/Ce/Zr catalyst resulted in altering the microstructure of the Cu particles. An increase in Cu concentration from 5 to 35 wt%, at a constant ZrO<sub>2</sub>/CeO<sub>2</sub> molar ratio of 1/1, resulted in an increase in crystallite size and consequently a decrease in the specific surface area of the active particles and a significant inhibition of CO production.

The increase in the hydrogen yield for modified catalysts can result from higher surface basicity of these catalysts. This is due to the fact that surface sites of higher basicity catalyze the reaction of ethanol dehydrogenation to acetaldehyde (2) [54,55].

During ethanol steam reforming, different types of carbon are being deposited on the catalyst surface, which is one of the reasons for catalyst deactivation [26,56]. This is strongly related with the reaction conditions and used catalysts. According to literature, carbon is formed during Boudouard reaction and dissociation of hydrocarbons molecules [57]. Various forms of carbon can be identified by peak positions in TPO profiles since amorphous carbon is oxidized at low temperature, whereas filamentous carbon undergoes oxidation at higher temperature (>823 K) [58]. The recorded TPO profiles are depicted in Figure 9. Based on the position of peak maxima (502–663 K), it can be stated that carbon deposit is in the amorphous state in the case of all catalysts [59].

In TPO profile for Cu/Zr, two separated CO<sub>2</sub> peaks of very small intensity can be visible with the maximum at 502 and 576 K. The amount of calculated carbon deposit is the smallest among spent catalyst and equal to 16.4 C<sub>S</sub> mg/g. The first peak of CO<sub>2</sub> is accompanied by peak of H<sub>2</sub>O, which is formed during oxidation (maximum at 507 K). The presence of water during oxidation suggests that carbon deposit contains also hydrogen. On the other hand, oxidation of remaining intermediates (C<sub>x</sub>H<sub>y</sub>O<sub>z</sub>), formed during ESR reaction, cannot be excluded since the temperature of oxidation is low [60]. The very low concentration of carbon for Cu/Zr catalyst results from its low activity in ethanol steam reforming. Similarly, water peak is observed for Cu/Zr/Ce catalyst but signal is shifted to higher temperature (557 K) and is of higher intensity in comparison with unmodified

catalyst. This is also valid for CO<sub>2</sub> signal with the maximum at 550 K. The increase in temperature of surface carbon oxidation is due to stronger carbon interaction with catalyst surface. The amount of carbon deposit is 79.5 mg C<sub>s</sub>/g, which is the highest recorded value among spent catalysts. The decrease in concentration of carbon deposit (63.0 mg C<sub>s</sub>/g) can be stated for Cu/Zr/Ni in comparison with Cu/Zr/Ce. In this case, there is also fraction of carbon that contains hydrogen since the peak of water during oxidation is present (569 K). Further shift of CO<sub>2</sub> peak toward higher temperature is visible in the case of Cu/Zr/Co catalyst. In the TPO profile of this catalyst, there are two separated CO<sub>2</sub> peaks at 579 and 663 K. Based on these two signals, the calculated concentration of surface carbon is equal to 49.1 mg C<sub>s</sub>/g. Moreover, the absence of H<sub>2</sub>O peaks proves that carbon deposit does not contain hydrogen and there is no oxidation of surface intermediates. For this catalyst, oxidation of carbon, which is formed on the surface during ethanol steam reforming, is hindered since CO<sub>2</sub> peaks emerge at the highest temperature when compared with the rest of spent catalysts.

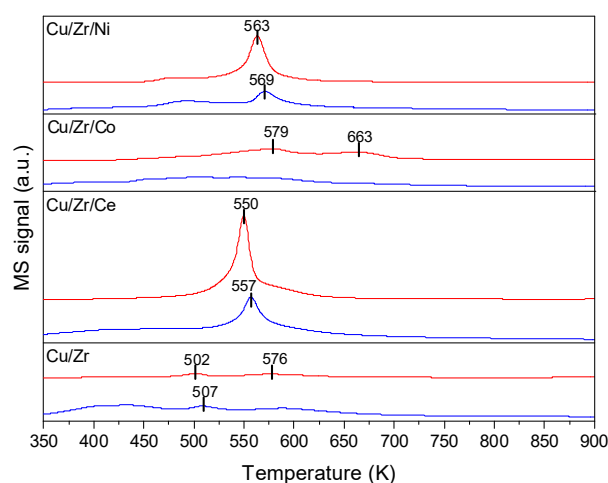


**Figure 9.** TPO profiles for spent catalysts: CO<sub>2</sub>—red line and H<sub>2</sub>O—blue line (signal multiplied by factor of 8).

The clear correlation between hydrogen yield and BET surface area or copper dispersion was not found.

### 3. Materials and Methods

#### 3.1. Materials

For the synthesis of catalysts, Ni(NO<sub>3</sub>)<sub>2</sub>·6H<sub>2</sub>O, Co(NO<sub>3</sub>)<sub>2</sub>·6H<sub>2</sub>O, Cu(NO<sub>3</sub>)<sub>2</sub>·3H<sub>2</sub>O, Ce(NO<sub>3</sub>)<sub>3</sub>·6H<sub>2</sub>O, and ZrO(NO<sub>3</sub>)<sub>2</sub>·H<sub>2</sub>O were purchased from Sigma–Aldrich USA (St. Louis, MO, USA); citric acid monohydrate was purchased from Stanlab Sp.j. Poland; and 65 mass% nitric acid was purchased from Avantor Performance Materials Poland; all the compounds and reagents were of AR grade. To determine the catalyst activity, ethanol of purity spectrophotometric grade, purchased from Merck KGaA was used.

#### 3.2. Catalysts Preparation

All precursors of Cu, Zr, Co, Ni, and Ce catalysts—oxides—have been prepared according to the method of thermal decomposition of organic complexes containing metallic components of catalyst [61]. Stoichiometric amounts of nitrates of Cu, Zr, Co, Ni, and Ce were carefully added, thoroughly stirred, to the solution of citric acid (concentration of 2 mol/dm<sup>3</sup>+2% excess). Then, the mixture was evaporated in a rotary vacuum evaporator in temperature of 363 K for around 24 h. The precipitate of formed citrates was carefully oxidized to prevent local overheating and explosive course of the oxidation reaction (temperature program: 360 K, 0.1 K/min; 403 K). The formed mixture of oxides was

calcined in a muffle with access of air (temperature program: 373, 473, 523, 573, and 623 K during 1 h).

The reason we used this method is perfectly mixed components thanks to the branched structure of citrates and consequently excellent homogeneity and fully repeatable properties of the prepared catalyst [62]. The conventional method of co-precipitation did not provide such results, although it is usually used, as it is described in the literature.

The last stages of preparation were pelletizing the resulting powder, crushing, and sizing (0.8–1 mm grain). In all obtained catalysts, the ratio of respective metals was about 63/34/4 (mass%/mass%/mass%). The composition of the reference Cu/Zr catalyst was equal to 63.8/36.2 (mass%/mass%) (Table 1).

### 3.3. Catalysts Characterization

Phase analysis based on the X-ray powder diffraction (XRD) measurements was performed on a X'PERT PRO MDP diffractometer with the X'CELERATOR detector, working in Bragg–Brentano geometry. The XRD measurements (at 40 kV and 30 mA) were performed in the  $2\theta$  range from  $5^\circ$  to  $90^\circ$  with the interpolated step size  $0.02^\circ$ . The crystallite sizes were calculated from Scherrer method. The XRD phase analysis was performed using reference standards from the International Centre for Diffraction Data (ICDD) PDF-4 database.

The BET surface area was measured with nitrogen adsorption at 77 K using Quantachrome Autosorb-1. Prior to the measurements, samples were preheated and degassed under vacuum at 373 K for 18 h. The pores size distribution profiles were obtained by Barrett–Joyner–Halenda (BJH) method from a desorption branch. The micropore area was obtained by V–t plot method.

The active surface of copper ( $S_{Cu}$ ) in the reduced catalyst was determined with the use of reactive adsorption of  $N_2O$  at 363 K (VG/Fisons Quartz 200D) according to the method described in [63]. It has been assumed in calculations that the reoxidation of surface copper follows the chemical equation:  $2Cu(s) + N_2O(g) \rightarrow Cu_2O(s) + N_2(g)$  and that  $1\text{ m}^2$  of elemental copper corresponds to  $6.1\text{ }\mu\text{mol}$  of  $O_2$ .

The  $H_2$ -TPR (temperature-programmed reduction of  $H_2$ ) measurements were performed in ChemBED-3000 (Quantachrome) u-shape quartz flow reactor (diameter ca. 5 mm) at temperature range of 300–1050 K with temperature ramp of 10 K/min and a flow rate of 5%  $H_2$  in Ar. Before the TPR analysis, all samples were kept in a stream of helium at 373 K for 1.5 h to remove physically adsorbed water.

The  $CO_2$ -TPD ( $CO_2$  temperature-programmed desorption) measurements were carried out in quartz fixed-bed flow reactor connected online to mass spectrometer (QMG 220 PRISMA PLUS). Prior to TPD run, sample (50 mg) was reduced in 5%  $H_2$ /Ar flow at 723 K for 1 h. Next, reactor was cooled down to room temperature (RT) and pulses (250  $\mu\text{L}$ ) of 5%  $CO_2$ /Ar were introduced until saturation. Then, sample was flashed with He flow (40 mL/min) for 0.5 h until obtaining stable  $CO_2$  line ( $m/z = 44$ ). TPD was done from RT to 973 K with  $\Delta T = 10\text{ K/min}$  under He flow.

The TPO (temperature-programmed oxidation measurements) of spent catalysts were performed using the same set-up line as for  $CO_2$ -TPD. For typical TPO run, 20 mg of sample was put in the reactor. Next, sample was oxidized in the stream of 5%  $O_2$ /He (30 mL/min) in the temperature range of RT–900 K. The following signals ( $m/z$ ) were monitored with QMS during TPO: 18 ( $H_2O$ ), 32 ( $O_2$ ), and 44 ( $CO_2$ ). The amount of deposited carbon ( $C_s$ ) was calculated for spent catalysts after time on stream = 50 h. It was assumed that entire carbon undergoes oxidation during TPO according to the following chemical equation:  $C_s + O_2 = CO_2$ . The oxidation of fraction of carbon that contained hydrogen was not taken into consideration. The calibration of  $CO_2$  mass spectrometer signal was performed by injecting pulses of 5%  $CO_2$ /He with sampling loop of 250  $\mu\text{L}$ .

### 3.4. Catalytic Tests

Catalytic experiments were performed in the continuous flow fixed-bed reactor of  $8\text{ cm}^3$  volume, made of stainless steel. To obtain the active form, the catalyst sample of 2 g

was reduced in a stream of diluted hydrogen (7 vol.% H<sub>2</sub> in N<sub>2</sub>) at temperature of 723 K at atmospheric pressure and stabilized in the mixture of reactants (temperature program: 443 K, 1.5 K/min; 553 K for 4 h). This procedure was repeated until the hydrogen yield was constant. Testing parameters were temperature range dependent on respective catalyst activity of 433–593 K, the reactant flow of 100 mL/min, and ethanol to water initial molar ratio of 1:3 in the stream of pure N<sub>2</sub>. Previously, the feed nitrogen was deoxidized with the BTS deoxidizer and dehydrated with the molecular sieve of 5 Å. The inlet and outlet gases were directed on-line to the gas chromatograph VARIAN STAR 3800. The gaseous products were analyzed in the system of Carbo Plot P7 column (25 m × 0.53 mm) and Supelcowax 10 column (30 m × 0.32 mm). Ethanol was determined quantitatively in the Supelcowax 10 column and FID detector, and the remaining gases were determined in the Carbo Plot P7 column and TCD detector. Additionally, carbon monoxide and methane were determined quantitatively in the methanizer with the sensitivity of 20 ppb.

Activity of tested catalysts was characterized by hydrogen yield, ethanol conversion, and selectivities of carbon monoxide and methane according to formulas given below [64]:

$$W_{\text{H}_2} = \frac{V_{\text{H}_2}}{m_{\text{cat}}}, \quad (\text{L}/\text{kg}_{\text{cat}} \cdot \text{h}) \quad (8)$$

$$\alpha = \frac{F_{\text{EtOH}}^{\text{in}} - F_{\text{EtOH}}^{\text{out}}}{F_{\text{EtOH}}^{\text{in}}} 100, \quad (\%) \quad (9)$$

$$S_i = \frac{F_i^{\text{out}}}{2(F_{\text{EtOH}}^{\text{in}} - F_{\text{EtOH}}^{\text{out}})} 100, \quad (\%), \quad (10)$$

where  $m_{\text{cat}}$  (g)—catalyst mass,  $V_{\text{H}_2}$  (L/h)—volume flow rate of hydrogen,  $F_i^{\text{in}}$  and  $F_i^{\text{out}}$  (mol/h)—molar flow rate of  $i$ -th component at input and output (CO, CH<sub>4</sub>), respectively, and EtOH - ethanol.

#### 4. Conclusions

The investigations on activity of tricomponent copper-based catalysts have been conducted, focusing on those applied in the ethanol steam reforming process. The properties of these catalysts were compared with those of the tested bicomponent Cu/Zr catalyst and prepared according to the same procedure. Relatively low reaction temperature using copper-based catalysts and very low value of carbon monoxide selectivity are important advantages. The disadvantage was not of sufficient value for hydrogen yield.

Among investigated Cu/Zr/Co, Cu/Zr/Ni, and Cu/Zr/Ce, the best performance was achieved for Cu/Zr/Ce catalyst. A hydrogen yield of 400 L/(kg<sub>cat</sub>·h) with ethanol conversion close to 100% with the lowest selectivity towards CO was obtained in the presence of this catalyst at 573 K. It must be highlighted that the selectivity towards carbon monoxide was below a value of 0.5%, required for use in fuel cells.

The addition of nickel to the Cu/Zr catalyst improved hydrogen yield to the highest value of 500 L/(kg<sub>cat</sub>·h), but unfortunately it generates large amounts of carbon monoxide (selectivity reached 27%) and methane (selectivity reached 36%). The addition of cobalt to the Cu/Zr catalyst caused increase in hydrogen yield similarly to that caused by the cerium addition. However, selectivity towards carbon monoxide was higher.

Further investigations on the application of Cu/Zr/Ce catalyst in the ethanol steam reforming process should be focused to wider analyses of the role and concentration of cerium.

**Author Contributions:** Conceptualization, M.M.-L. and Ł.H.; methodology, M.M.-L.; investigation, Ł.H., M.Ś., K.S. and M.R.-M.; data curation, Ł.H., M.M.-L., M.K., M.Ś., K.S. and M.R.-M.; writing—original draft preparation, Ł.H., M.M.-L., M.K.; writing—review and editing, Ł.H., M.M.-L., M.K., M.Ś.; supervision, M.M.-L., M.K. All authors have read and agreed to the published version of the manuscript.

**Funding:** The work was in part supported by National Science Center within the project SONATA, No: 2016/23/D/ST4/02492, 2017-2020 (M.Ś).

**Data Availability Statement:** Institute of Chemical Engineering, Polish Academy of Sciences, 5 Bałtycka Street, 44-100 Gliwice, Poland and Jerzy Haber Institute of Catalysis and Surface Chemistry, Polish Academy of Sciences, 8 Niezapominajek Street, 30-239 Krakow, Poland.

**Conflicts of Interest:** The authors declare no conflict of interest.

## References

1. Ogo, S.; Sekine, Y. Recent progress in ethanol steam reforming using non-noble transition metal catalysts: A review. *Fuel Process. Technol.* **2020**, *199*, 106238–106249. [[CrossRef](#)]
2. Gonzalez-Gil, R.; Chamorro-Burgos, I.; Herrera, C.; Larrubia, M.A.; Laborde, M.; Marino, F.; Alemany, L.J. Production of hydrogen by catalytic steam reforming of oxygenated model compounds on Ni-modified supported catalysts. Simulation and experimental study. *Int. J. Hydrogen Energy* **2015**, *40*, 11217–11227. [[CrossRef](#)]
3. Madej-Lachowska, M.; Kulawska, M.; Słoczyński, J. Methanol as a high purity hydrogen source for fuel cells: A brief review of catalysts and rate expressions. *Chem. Proc. Eng.* **2017**, *38*, 147–162. [[CrossRef](#)]
4. Rashid, M.M.; Al Mesfer, M.K.; Naseem, H.; Danish, M. Hydrogen Production by Water Electrolysis: A Review of Alkaline Water Electrolysis, PEM Water Electrolysis and High Temperature Water Electrolysis. *Int. J. Eng. Adv. Technol.* **2015**, *4*, 80–93.
5. Luo, M.; Yi, Y.; Wang, S.; Wang, Z.; Du, M.; Pan, J.; Wang, Q. Review of hydrogen production using chemical-looping technology. *Renew. Sustain. Energy Rev.* **2018**, *81*, 3186–3214. [[CrossRef](#)]
6. Li, Y.; Zhang, Z.; Jia, P.; Dong, D.; Wang, Y.; Hu, S.; Xiang, J.; Liu, Q.; Hu, X. Ethanol steam reforming over cobalt catalysts: Effect of a range of additives on the catalytic behaviors. *J. Energy Inst.* **2020**, *93*, 165–184. [[CrossRef](#)]
7. Vizcaino, A.J.; Carrero, A.; Calles, J.A. Hydrogen production by ethanol steam reforming over Cu–Ni supported catalysts. *Int. J. Hydrogen Energy* **2007**, *32*, 1450–1461. [[CrossRef](#)]
8. Snytnikov, P.V.; Badmaev, S.D.; Volkova, G.G.; Potemkin, D.I.; Zyryanova, M.M.; Belyaev, V.D. Catalysts for hydrogen production in a multifuel processor by methanol, dimethyl ether and bioethanol steam reforming for fuel cell applications. *Int. J. Hydrogen Energy* **2012**, *37*, 16388–16396. [[CrossRef](#)]
9. Moraes, T.S.; Borges, L.E.P.; Farrauto, R.; Noronha, F.B. Steam reforming of ethanol on Rh/SiCeO<sub>2</sub> washcoated monolith catalyst: Stable catalyst performance. *Int. J. Hydrogen Energy* **2018**, *43*, 115–126. [[CrossRef](#)]
10. Palma, V.; Castaldo, F.; Ciambelli, P.; Iaquaniello, G. H<sub>2</sub> Production for MC Fuel Cell by Steam Reforming of Ethanol Over MgO Supported Pd, Rh, Ni and Co Catalysts. *Appl. Catal. B Environ.* **2014**, *145*, 73–84. [[CrossRef](#)]
11. Jia, H.; Zhang, J.; Yu, J.; Yang, X.; Sheng, X.; Xu, H.; Sun, C.; Shen, W.; Goldbach, A. Efficient H<sub>2</sub> production via membrane-assisted ethanol steam reforming over Ir/CeO<sub>2</sub> catalyst. *Int. J. Hydrogen Energy* **2019**, *44*, 24733–24745. [[CrossRef](#)]
12. Morales, M.; Segarra, M. Steam reforming and oxidative steam reforming of ethanol over La<sub>0.6</sub>Sr<sub>0.4</sub>CoO<sub>3-δ</sub> perovskite as catalyst precursor for hydrogen production. *Appl. Catal. A Gen.* **2015**, *502*, 305–311. [[CrossRef](#)]
13. Liu, F.; Qu, Y.; Yue, Y.; Liu, G.; Liu, Y. Nano bimetallic alloy of Ni-Co obtained from LaCo<sub>x</sub>Ni<sub>1-x</sub>O<sub>3</sub> and its catalytic performance for steam reforming of ethanol. *RSC Adv.* **2015**, *5*, 16837–16916.
14. Moraes, T.S.; Neto, R.C.R.; Ribeiro, M.C.; Mattos, L.V.; Kourtelesis, M.; Ladas, S. The study of the performance of PtNi/CeO<sub>2</sub>-nanocube catalysts for low temperature steam reforming of ethanol. *Catal. Today* **2015**, *242*, 35–49. [[CrossRef](#)]
15. Chiou, J.Y.Z.; Lee, C.-L.; Ho, K.-F.; Huang, H.-H.; Yu, S.-W.; Wang, C.-B. Catalytic performance of Pt-promoted cobalt-based catalysts for the steam reforming of ethanol. *Int. J. Hydrogen Energy* **2014**, *39*, 5653–5662. [[CrossRef](#)]
16. Wang, F.; Cai, W.; Provendier, H.; Schuurman, Y.; Descorme, C.; Mirodatos, C. Hydrogen production from ethanol steam reforming over Ir/CeO<sub>2</sub> catalysts: Enhanced stability by PrO<sub>x</sub> promotion. *Int. J. Hydrogen Energy* **2011**, *36*, 13566–13574. [[CrossRef](#)]
17. Hamryszak, Ł.; Madej-Lachowska, M.; Kulawska, M.; Ruggiero-Mikołajczyk, M.; Samson, K.; Śliwa, M. Investigation on binary copper-based catalysts used in the ethanol steam reforming process. *React. Kinet. Catal. Mech.* **2020**, *130*, 727–739. [[CrossRef](#)]
18. Fajardo, H.V.; Longo, E.; Mezalira, D.; Nuernberg, G.; Almerindo, G.; Collasiol, A.; Probst, L.F.D.; Garcia, I.T.S.; Carreño, N.L.V. Influence of support on catalytic behavior of nickel catalysts in the steam reforming of ethanol for hydrogen production. *Environ. Chem. Lett.* **2010**, *8*, 79–85. [[CrossRef](#)]
19. Araiza, D.G.; Gómez-Cortés, A.; Díaz, G. Effect of ceria morphology on the carbon deposition during steam reforming of ethanol over Ni/CeO<sub>2</sub> catalysts. *Catal. Today* **2020**, *349*, 235–243. [[CrossRef](#)]
20. Fatsikostas, A.N.; Kondarides, D.I.; Verykios, X.E. Production of hydrogen for fuel cells by reformation of biomass-derived ethanol. *Catal. Today* **2002**, *75*, 145–155. [[CrossRef](#)]
21. Rossetti, I.; Lasso, J.; Finocchio, E.; Ramis, G.; Nichele, V.; Signoretto, M.; Di Michele, A. TiO<sub>2</sub>-supported catalysts for the steam reforming of ethanol. *Appl. Catal. A Gen.* **2014**, *477*, 42–53. [[CrossRef](#)]
22. Pinton, N.; Vidal, M.V.; Signoretto, M.; Martínez-Arias, A.; Cortés Corberán, V. Ethanol steam reforming on nanostructured catalysts of Ni, Co and CeO<sub>2</sub>: Influence of synthesis method on activity, deactivation and regenerability. *Catal. Today* **2017**, *296*, 135–143. [[CrossRef](#)]
23. Li, S.; Li, M.; Zhang, C.; Wang, S.; Ma, X.; Gong, J. Steam reforming of ethanol over Ni/ZrO<sub>2</sub> catalysts: Effect of support on product distribution. *Int. J. Hydrogen Energy* **2012**, *37*, 2940–2949. [[CrossRef](#)]

24. Bergamaschi, V.S.; Carvalho, F.M.S.; Rodrigues, C.; Fernandes, D.B. Preparation and evaluation of zirconia microspheres as inorganic exchanger in adsorption of copper and nickel ions and as catalyst in hydrogen production from bioethanol. *Chem. Eng. J.* **2005**, *112*, 153–158. [[CrossRef](#)]
25. Ni, M.; Leung, D.Y.C.; Leung, M.K.H. A review on reforming bio-ethanol for hydrogen production. *Int. J. Hydrogen Energy* **2007**, *32*, 3238–3247. [[CrossRef](#)]
26. Sharma, Y.C.; Kumar, A.; Prasad, R.; Upadhyay, S.N. Ethanol steam reforming for hydrogen production: Latest and effective catalyst modification strategies to minimize carbonaceous deactivation. *Renew. Sustain. Energy Rev.* **2017**, *74*, 89–103. [[CrossRef](#)]
27. Madej-Lachowska, M.; Moroz, H.; Wyzgoł, H.; Hamryszak, Ł. The investigation of activity the bimetallic catalysts based on nickel oxide, cobalt oxide, cerium oxide in ethanol steam reforming (ESR). In *Research Papers of the Institute of Chemical Engineering*; Polish Academy of Sciences: Warsaw, Poland, 2017; Volume 21, pp. 99–117.
28. Batista, M.S.; Santos, R.K.S.; Assaf, E.M.; Assaf, J.M.; Ticianelli, E.A. High efficiency steam reforming of ethanol by cobalt-based catalysts. *J. Power Sources* **2004**, *134*, 27–32. [[CrossRef](#)]
29. Augusto, B.L.; Ribeiro, M.C.; Aires, F.J.C.S.; da Silva, V.T.; Noronha, F.B. Hydrogen production by the steam reforming of ethanol over cobalt catalysts supported on different carbon nanostructures. *Catal. Today* **2020**, *344*, 66–74. [[CrossRef](#)]
30. Greluk, M.; Rotko, M.; Słowik, G.; Turczyniak-Surdacka, S. Hydrogen production by steam reforming of ethanol over Co/CeO<sub>2</sub> catalysts: Effect of cobalt content. *J. Energy Inst.* **2019**, *92*, 222–238. [[CrossRef](#)]
31. Kulawska, M.; Madej-Lachowska, M.; Hamryszak, Ł.; Moroz, H.; Wyzgoł, H. Application of copper catalyst to the hydrogen production by steam reforming of ethanol. *Przem. Chem.* **2019**, *98*, 1992–1995.
32. de Lima, S.M.; Silva, A.M.; Graham, U.M.; Jacobs, G.; Davis, B.H.; Mattos, L.V. Ethanol decomposition and steam reforming of ethanol over CeZrO<sub>2</sub> and Pt/CeZrO<sub>2</sub> catalyst: Reaction mechanism and deactivation. *Appl. Catal. A Gen.* **2009**, *352*, 95–113. [[CrossRef](#)]
33. Dan, M.; Mihet, M.; Tasnadi-Asztalos, Z.; Imre-Lucaci, A.; Katona, G.; Lazar, M.D. Hydrogen production by ethanol steam reforming on nickel catalysts: Effect of support modification by CeO<sub>2</sub> and La<sub>2</sub>O<sub>3</sub>. *Fuel* **2015**, *147*, 260–268. [[CrossRef](#)]
34. Montero, C.; Remiro, A.; Arandia, A.; Benito, P.L.; Bilbao, J.; Gayubo, A.G. Reproducible performance of a Ni/La<sub>2</sub>O<sub>3</sub>-αAl<sub>2</sub>O<sub>3</sub> catalyst in ethanol steam reforming under reaction–regeneration cycles. *Fuel Process. Technol.* **2016**, *152*, 215–222. [[CrossRef](#)]
35. Xiao, Z.; Wu, C.; Wang, L.; Xu, J.; Zheng, Q.; Pan, L.; Zou, J.; Zhang, X.; Li, G. Boosting hydrogen production from steam reforming of ethanol on nickel by lanthanum doped ceria. *Appl. Catal. B Environ.* **2021**, *286*, 119884–119897. [[CrossRef](#)]
36. Kim, D.; Kwak, B.S.; Park, N.-K.; Han, G.B.; Kang, M. Dynamic hydrogen production from ethanol steam-reforming reaction on Ni<sub>x</sub>M<sub>1-x</sub>O<sub>y</sub>/SBA-15 catalytic system. *Int. J. Energy Res.* **2015**, *39*, 279–292. [[CrossRef](#)]
37. Barroso, M.N.; Gomez, M.F.; Arrua, L.A.; Abello, M.C. Hydrogen production by ethanol reforming over NiZnAl catalysts. *Appl. Catal. A Gen.* **2006**, *304*, 116–123. [[CrossRef](#)]
38. Anjaneyulu, C.; da Costa, L.O.O.; Ribeiro, M.C.; Rabelo-Neto, R.C.; Mattos, L.V.; Venugopal, A.; Noronha, F.B. Effect of Zn addition on the performance of Ni/Al<sub>2</sub>O<sub>3</sub> catalyst for steam reforming of ethanol. *Appl. Catal. A Gen.* **2016**, *519*, 85–98. [[CrossRef](#)]
39. Fang, W.; Paul, S.; Capron, M.; Biradar, A.V.; Umbarkar, S.B.; Dongare, M.K. Highly loaded well dispersed stable Ni species in Ni<sub>x</sub>Mg<sub>2</sub>AlO<sub>y</sub> nanocomposites: Application to hydrogen production from bioethanol. *Appl. Catal. B Environ.* **2015**, *166*, 485–496. [[CrossRef](#)]
40. Sohrabi, S.; Irankhah, A. Synthesis, characterization, and catalytic activity of Ni/CeMnO<sub>2</sub> catalysts promoted by copper, cobalt, potassium and iron for ethanol steam reforming. *Int. J. Hydrogen Energy* **2021**, *46*, 12846–12856. [[CrossRef](#)]
41. Das, N.K.; Dalai, A.K.; Ranganathan, R. Hydrogen Yield from Low Temperature Steam Reforming of Ethanol. *Can. J. Chem. Eng.* **2007**, *85*, 92–100. [[CrossRef](#)]
42. Śliwa, M.; Samson, K. Steam reforming of ethanol over copper-zirconia based catalysts doped with Mn, Ni, Ga. *Int. J. Hydrogen Energy* **2021**, *46*, 555–564. [[CrossRef](#)]
43. Dancini-Pontes, I.; DeSouza, M.; Silva, F.A.; Scaliante, M.H.N.O.; Alonso, C.G.; Bianchi, G.S.; Neto, A.M.; Pereira, G.M.; Fernandes-Machado, N.R.C. Influence of the CeO<sub>2</sub> and Nb<sub>2</sub>O<sub>5</sub> supports and the inert gas in ethanol steam reforming for H<sub>2</sub> production. *Chem. Eng. J.* **2015**, *273*, 66–74. [[CrossRef](#)]
44. Chen, L.-C.; Lin, S.D. Effects of the pretreatment of CuNi/SiO<sub>2</sub> on ethanol steam reforming: Influence of bimetal morphology. *Appl. Catal. B Environ.* **2014**, *148–149*, 509–519. [[CrossRef](#)]
45. Donga, X.-F.; Zoub, H.-B.; Lin, W.-M. Effect of preparation conditions of CuO-CeO<sub>2</sub>-ZrO<sub>2</sub> catalyst on CO removal from hydrogen-rich gas. *Int. J. Hydrogen Energy* **2006**, *31*, 2337–2344. [[CrossRef](#)]
46. Ziółek, M.; Nowak, I. *Kataliza Heterogeniczna–Wybrane Zagadnienia*; Wydawnictwo Naukowe UAM: Poznań, Poland, 1999.
47. Bahari, M.B.; Phuc, N.H.H.; Abdullah, B.; Alenazey, F.; Vo, D.-V.N. Ethanol dry reforming for syngas production over Ce-promoted Ni/Al<sub>2</sub>O<sub>3</sub> catalyst. *J. Environ. Chem. Eng.* **2016**, *4*, 4830–4838. [[CrossRef](#)]
48. Basahel, S.N.; Mokhtar, M.; Alsharaeh, E.H.; Ali, T.T.; Mahmoud, H.A.; Narasimharao, K. Physico-Chemical and Catalytic Properties of Mesoporous CuO-ZrO<sub>2</sub> Catalysts. *Catalysts* **2016**, *6*, 57–77. [[CrossRef](#)]
49. Gao, P.; Li, F.; Zhan, H.J.; Zhao, N.; Xiao, F.K.; Wei, W.; Zhong, L.S.; Wang, H.; Sun, Y.H. Influence of Zr on the performance of Cu/Zn/Al/Zr catalysts via hydrotalcite-like precursors for CO<sub>2</sub> hydrogenation to methanol. *J. Catal.* **2013**, *298*, 51–60. [[CrossRef](#)]
50. Díez, V.K.; Apesteguía, C.R.; Di Cosimo, J.I. Acid–base properties and active site requirements for elimination reactions on alkali-promoted MgO catalysts. *Catal. Today* **2000**, *63*, 53–62. [[CrossRef](#)]

51. Baneshi, J.; Haghighi, M.; Jodeiri, N.; Abdollahifar, M.; Ajamein, H. Homogeneous precipitation synthesis of CuO–ZrO<sub>2</sub>–CeO<sub>2</sub>–Al<sub>2</sub>O<sub>3</sub> nanocatalyst used in hydrogen production via methanol steam reforming for fuel cell applications. *Energy Convers. Manage.* **2014**, *87*, 928–937. [[CrossRef](#)]
52. Wang, G.; Zuo, Y.; Han, M.; Wang, J. Copper crystallite size and methanol synthesis catalytic property of Cu-based catalysts promoted by Al, Zr and Mn. *Reac. Kinet. Mech. Cat.* **2010**, *101*, 443–454. [[CrossRef](#)]
53. Mastalir, A.; Frank, B.; Szizybalski, A.; Soerijanto, H.; Deshpande, A.; Niederberger, M.; Schomäcker, R.; Schlögl, R.; Ressler, T. Steam reforming of methanol over Cu/ZrO<sub>2</sub>/CeO<sub>2</sub> catalysts: A kinetic study. *J. Catal.* **2005**, *230*, 464–475. [[CrossRef](#)]
54. Binet, C.; Daturi, M.; Lavalley, J.C. IR study of polycrystalline ceria properties in oxidised and reduced states. *Catal. Today* **1999**, *50*, 207–225. [[CrossRef](#)]
55. Ebiad, M.A.; Abd El-Hafiz, D.R.; Elsalamony, R.A.; Mohamed, L.S. Ni supported high surface area CeO<sub>2</sub>–ZrO<sub>2</sub> catalysts for hydrogen production from ethanol steam reforming. *RSC Adv.* **2012**, *2*, 8145–8156. [[CrossRef](#)]
56. Wang, J.H.; Lee, C.S.; Lin, M.C. Mechanism of ethanol reforming: Theoretical foundations. *J. Phys. Chem. C.* **2009**, *113*, 6681–6688. [[CrossRef](#)]
57. Mattos, L.V.; Jacobs, G.; Davis, B.H.; Noronha, F.B. Production of hydrogen from ethanol: Review of reaction mechanism and catalyst deactivation. *Chem. Rev.* **2012**, *112*, 4094–4123. [[CrossRef](#)] [[PubMed](#)]
58. Song, J.H.; Yoo, S.; Yoo, J.; Park, S.; Gim, M.Y.; Kim, T.H.; Song, I.K. Hydrogen production by steam reforming of ethanol over Ni/Al<sub>2</sub>O<sub>3</sub>–La<sub>2</sub>O<sub>3</sub> xerogel catalysts. *Mol. Catal.* **2017**, *434*, 123–133. [[CrossRef](#)]
59. Sharma, P.K.; Saxena, N.; Bhatt, A.; Rajagopal, C.; Roy, P.K. Synthesis of mesoporous bimetallic Ni–Cu catalysts supported over ZrO<sub>2</sub> by a homogenous urea coprecipitation method for catalytic steam reforming of ethanol. *Catal. Sci. Technol.* **2013**, *3*, 1017–1026. [[CrossRef](#)]
60. Cai, W.; Wang, F.; Zhan, E.; Van Veen, A.C.; Mirodatos, C.; Shen, W. Hydrogen production from ethanol over Ir/CeO<sub>2</sub> catalysts: A comparative study of steam reforming, partial oxidation and oxidative steam reforming. *J. Catal.* **2008**, *257*, 96–107. [[CrossRef](#)]
61. Courty, P.; Ajoy, H.; Marcilly, C.; Delmon, B. Oxydesmixtes en solution solide sous forme très divisée obtenus par décomposition thermique de précurseurs amorphes. *Powder Technol.* **1973**, *7*, 21–38. [[CrossRef](#)]
62. Lachowska, M. Steam reforming of methanol over Cu/Zn/Zr/Ga catalyst: Effect of the reduction conditions on the catalytic performance. *Reac. Kinet. Mech. Cat.* **2010**, *101*, 85–91. [[CrossRef](#)]
63. Żelazny, A.; Samson, K.; Grabowski, R.; Śliwa, M.; Ruggiero-Mikołajczyk, M.; Kornas, A. Hydrogenolysis of glycerol to propylene glycol over Cu/oxide catalysts: Influence of the support and reaction conditions. *Reac. Kinet. Mech. Cat.* **2017**, *121*, 329–343. [[CrossRef](#)]
64. Szarawara, J.; Skrzypek, J.; Gawdzik, A. *Podstawy Inżynierii Reaktorów Chemicznych*, 2nd ed.; WNT: Warsaw, Poland, 1991; pp. 20–45.